

Stringent Tests of Lorentz Invariance Violation from LHAASO Observations of GRB 221009A

Zhen Cao,^{1,2,3} F. Aharonian,^{4,5} Axikegu,⁶ Y.X. Bai,^{1,3} Y.W. Bao,⁷ D. Bastieri,⁸ X.J. Bi,^{1,2,3} Y.J. Bi,^{1,3} W. Bian,⁹ A.V. Bukevich,¹⁰ Q. Cao,¹¹ W.Y. Cao,¹² Zhe Cao,^{13,12} J. Chang,¹⁴ J.F. Chang,^{1,3,13} A.M. Chen,⁹ E.S. Chen,^{1,2,3} H.X. Chen,¹⁵ Liang Chen,¹⁶ Lin Chen,⁶ Long Chen,⁶ M.J. Chen,^{1,3} M.L. Chen,^{1,3,13} Q.H. Chen,⁶ S. Chen,¹⁷ S.H. Chen,^{1,2,3} S.Z. Chen,^{1,3} T.L. Chen,¹⁸ Y. Chen,⁷ N. Cheng,^{1,3} Y.D. Cheng,^{1,2,3} M.Y. Cui,¹⁴ S.W. Cui,¹¹ X.H. Cui,¹⁹ Y.D. Cui,²⁰ B.Z. Dai,¹⁷ H.L. Dai,^{1,3,13} Z.G. Dai,¹² Danzengluobu,¹⁸ X.Q. Dong,^{1,2,3} K.K. Duan,¹⁴ J.H. Fan,⁸ Y.Z. Fan,¹⁴ J. Fang,¹⁷ J.H. Fang,¹⁵ K. Fang,^{1,3} C.F. Feng,²¹ H. Feng,¹ L. Feng,¹⁴ S.H. Feng,^{1,3} X.T. Feng,²¹ Y. Feng,¹⁵ Y.L. Feng,¹⁸ S. Gabicci,²² B. Gao,^{1,3} C.D. Gao,²¹ Q. Gao,¹⁸ W. Gao,^{1,3} W.K. Gao,^{1,2,3} M.M. Ge,¹⁷ L.S. Geng,^{1,3} G. Giacinti,⁹ G.H. Gong,²³ Q.B. Gou,^{1,3} M.H. Gu,^{1,3,13} F.L. Guo,¹⁶ X.L. Guo,⁶ Y.Q. Guo,^{1,3} Y.Y. Guo,¹⁴ Y.A. Han,²⁴ M. Hasan,^{1,2,3} H.H. He,^{1,2,3} H.N. He,¹⁴ J.Y. He,¹⁴ Y. He,⁶ Y.K. Hor,²⁰ B.W. Hou,^{1,2,3} C. Hou,^{1,3} X. Hou,²⁵ H.B. Hu,^{1,2,3} Q. Hu,^{12,14} S.C. Hu,^{1,3,26} D.H. Huang,⁶ T.Q. Huang,^{1,3} W.J. Huang,²⁰ X.T. Huang,²¹ X.Y. Huang,¹⁴ Y. Huang,^{1,2,3} X.L. Ji,^{1,3,13} H.Y. Jia,⁶ K. Jia,²¹ K. Jiang,^{13,12} X.W. Jiang,^{1,3} Z.J. Jiang,¹⁷ M. Jin,⁶ M.M. Kang,²⁷ I. Karpikov,¹⁰ D. Kuleshov,¹⁰ K. Kurinov,¹⁰ B.B. Li,¹¹ C.M. Li,⁷ Cheng Li,^{13,12} Cong Li,^{1,3} D. Li,^{1,2,3} F. Li,^{1,3,13} H.B. Li,^{1,3} H.C. Li,^{1,3} Jian Li,¹² Jie Li,^{1,3,13} K. Li,^{1,3} S.D. Li,^{16,2} W.L. Li,²¹ W.L. Li,⁹ X.R. Li,^{1,3} Xin Li,^{13,12} Y.Z. Li,^{1,2,3} Zhe Li,^{1,3} Zhuo Li,²⁸ E.W. Liang,²⁹ Y.F. Liang,²⁹ S.J. Lin,²⁰ B. Liu,¹² C. Liu,^{1,3} D. Liu,²¹ D.B. Liu,⁹ H. Liu,⁶ H.D. Liu,²⁴ J. Liu,^{1,3} J.L. Liu,^{1,3} M.Y. Liu,¹⁸ R.Y. Liu,⁷ S.M. Liu,⁶ W. Liu,^{1,3} Y. Liu,⁸ Y.N. Liu,²³ Q. Luo,²⁰ Y. Luo,⁹ H.K. Lv,^{1,3} B.Q. Ma,²⁸ L.L. Ma,^{1,3} X.H. Ma,^{1,3} J.R. Mao,²⁵ Z. Min,^{1,3} W. Mitthumsiri,³⁰ H.J. Mu,²⁴ Y.C. Nan,^{1,3} A. Neronov,²² L.J. Ou,⁸ P. Pattarakijwanich,³⁰ Z.Y. Pei,⁸ J.C. Qi,^{1,2,3} M.Y. Qi,^{1,3} B.Q. Qiao,^{1,3} J.J. Qin,¹² A. Raza,^{1,2,3} D. Ruffolo,³⁰ A. Sáiz,³⁰ M. Saeed,^{1,2,3} D. Semikoz,²² L. Shao,¹¹ O. Shchegolev,^{10,31} X.D. Sheng,^{1,3} F.W. Shu,³² H.C. Song,²⁸ Yu.V. Stenkin,^{10,31} V. Stepanov,¹⁰ Y. Su,¹⁴ D.X. Sun,^{12,14} Q.N. Sun,⁶ X.N. Sun,²⁹ Z.B. Sun,³³ J. Takata,³⁴ P.H.T. Tam,²⁰ Q.W. Tang,³² R. Tang,⁹ Z.B. Tang,^{13,12} W.W. Tian,^{2,19} C. Wang,³³ C.B. Wang,⁶ G.W. Wang,¹² H.G. Wang,⁸ H.H. Wang,²⁰ J.C. Wang,²⁵ Kai Wang,⁷ Kai Wang,³⁴ L.P. Wang,^{1,2,3} L.Y. Wang,^{1,3} P.H. Wang,⁶ R. Wang,²¹ W. Wang,²⁰ X.G. Wang,²⁹ X.Y. Wang,⁷ Y. Wang,⁶ Y.D. Wang,^{1,3} Y.J. Wang,^{1,3} Z.H. Wang,²⁷ Z.X. Wang,¹⁷ Zhen Wang,⁹ Zheng Wang,^{1,3,13} D.M. Wei,¹⁴ J.J. Wei,¹⁴ Y.J. Wei,^{1,2,3} T. Wen,¹⁷ C.Y. Wu,^{1,3} H.R. Wu,^{1,3} Q.W. Wu,³⁴ S. Wu,^{1,3} X.F. Wu,¹⁴ Y.S. Wu,¹² S.Q. Xi,^{1,3} J. Xia,^{12,14} G.M. Xiang,^{16,2} D.X. Xiao,¹¹ G. Xiao,^{1,3} Y.L. Xin,⁶ Y. Xing,¹⁶ D.R. Xiong,²⁵ Z. Xiong,^{1,2,3} D.L. Xu,⁹ R.F. Xu,^{1,2,3} R.X. Xu,²⁸ W.L. Xu,²⁷ L. Xue,²¹ D.H. Yan,¹⁷ J.Z. Yan,¹⁴ T. Yan,^{1,3} C.W. Yang,²⁷ C.Y. Yang,²⁵ F. Yang,¹¹ F.F. Yang,^{1,3,13} L.L. Yang,²⁰ M.J. Yang,^{1,3} R.Z. Yang,¹² W.X. Yang,⁸ Y.H. Yao,^{1,3} Z.G. Yao,^{1,3} L.Q. Yin,^{1,3} N. Yin,²¹ X.H. You,^{1,3} Z.Y. You,^{1,3} Y.H. Yu,¹² Q. Yuan,¹⁴ H. Yue,^{1,2,3} H.D. Zeng,¹⁴ T.X. Zeng,^{1,3,13} W. Zeng,¹⁷ M. Zha,^{1,3} B.B. Zhang,⁷ F. Zhang,⁶ H. Zhang,⁹ H.M. Zhang,⁷ H.Y. Zhang,^{1,3} J.L. Zhang,¹⁹ Li Zhang,¹⁷ P.F. Zhang,¹⁷ P.P. Zhang,^{12,14} R. Zhang,^{12,14} S.B. Zhang,^{2,19} S.R. Zhang,¹¹ S.S. Zhang,^{1,3} X. Zhang,⁷ X.P. Zhang,^{1,3} Y.F. Zhang,⁶ Yi Zhang,^{1,14} Yong Zhang,^{1,3} B. Zhao,⁶ J. Zhao,^{1,3} L. Zhao,^{13,12} L.Z. Zhao,¹¹ S.P. Zhao,¹⁴ X.H. Zhao,²⁵ F. Zheng,³³ W.J. Zhong,⁷ B. Zhou,^{1,3} H. Zhou,⁹ J.N. Zhou,¹⁶ M. Zhou,³² P. Zhou,⁷ R. Zhou,²⁷ X.X. Zhou,^{1,2,3} X.X. Zhou,⁶ B.Y. Zhu,^{12,14} C.G. Zhu,²¹ F.R. Zhu,⁶ H. Zhu,¹⁹ K.J. Zhu,^{1,2,3,13} Y.C. Zou,³⁴ and X. Zuo^{1,3}

(The LHAASO Collaboration)*

¹Key Laboratory of Particle Astrophysics & Experimental Physics Division & Computing Center, Institute of High Energy Physics, Chinese Academy of Sciences, 100049 Beijing, China

²University of Chinese Academy of Sciences, 100049 Beijing, China

³Tianfu Cosmic Ray Research Center, 610000 Chengdu, Sichuan, China

⁴Dublin Institute for Advanced Studies, 31 Fitzwilliam Place, 2 Dublin, Ireland

⁵Max-Planck-Institut für Nuclear Physics, P.O. Box 103980, 69029 Heidelberg, Germany

⁶School of Physical Science and Technology & School of Information Science and Technology, Southwest Jiaotong University, 610031 Chengdu, Sichuan, China

⁷School of Astronomy and Space Science, Nanjing University, 210023 Nanjing, Jiangsu, China

⁸Center for Astrophysics, Guangzhou University, 510006 Guangzhou, Guangdong, China

⁹Tsung-Dao Lee Institute & School of Physics and Astronomy, Shanghai Jiao Tong University, 200240 Shanghai, China

¹⁰Institute for Nuclear Research of Russian Academy of Sciences, 117312 Moscow, Russia

¹¹Hebei Normal University, 050024 Shijiazhuang, Hebei, China

¹²University of Science and Technology of China, 230026 Hefei, Anhui, China

¹³State Key Laboratory of Particle Detection and Electronics, China

¹⁴Key Laboratory of Dark Matter and Space Astronomy & Key Laboratory of Radio Astronomy, Purple Mountain Observatory, Chinese Academy of Sciences, 210023 Nanjing, Jiangsu, China

¹⁵Research Center for Astronomical Computing, Zhejiang Laboratory, 311121 Hangzhou, Zhejiang, China

¹⁶Key Laboratory for Research in Galaxies and Cosmology, Shanghai Astronomical Observatory, Chinese Academy of Sciences, 200030 Shanghai, China

¹⁷School of Physics and Astronomy, Yunnan University, 650091 Kunming, Yunnan, China

¹⁸Key Laboratory of Cosmic Rays (Tibet University), Ministry of Education, 850000 Lhasa, Tibet, China

¹⁹National Astronomical Observatories, Chinese Academy of Sciences, 100101 Beijing, China

²⁰*School of Physics and Astronomy (Zhuhai) & School of Physics (Guangzhou)
& Sino-French Institute of Nuclear Engineering and Technology (Zhuhai),
Sun Yat-sen University, 519000 Zhuhai & 510275 Guangzhou, Guangdong, China*

²¹*Institute of Frontier and Interdisciplinary Science, Shandong University, 266237 Qingdao, Shandong, China*

²²*APC, Université Paris Cité, CNRS/IN2P3, CEA/IRFU, Observatoire de Paris, 119 75205 Paris, France*

²³*Department of Engineering Physics, Tsinghua University, 100084 Beijing, China*

²⁴*School of Physics and Microelectronics, Zhengzhou University, 450001 Zhengzhou, Henan, China*

²⁵*Yunnan Observatories, Chinese Academy of Sciences, 650216 Kunming, Yunnan, China*

²⁶*China Center of Advanced Science and Technology, Beijing 100190, China*

²⁷*College of Physics, Sichuan University, 610065 Chengdu, Sichuan, China*

²⁸*School of Physics, Peking University, 100871 Beijing, China*

²⁹*Guangxi Key Laboratory for Relativistic Astrophysics,*

School of Physical Science and Technology, Guangxi University, 530004 Nanning, Guangxi, China

³⁰*Department of Physics, Faculty of Science, Mahidol University, Bangkok 10400, Thailand*

³¹*Moscow Institute of Physics and Technology, 141700 Moscow, Russia*

³²*Center for Relativistic Astrophysics and High Energy Physics,*

School of Physics and Materials Science & Institute of Space Science and Technology,

Nanchang University, 330031 Nanchang, Jiangxi, China

³³*National Space Science Center, Chinese Academy of Sciences, 100190 Beijing, China*

³⁴*School of Physics, Huazhong University of Science and Technology, Wuhan 430074, Hubei, China*

(Dated: February 12, 2024)

Very recently, the Large High Altitude Air Shower Observatory (LHAASO) reported the observation of the very early TeV afterglow of the brightest-of-all-time GRB 221009A, recording the highest photon statistics in the TeV band ever from a gamma-ray burst. We use this unique observation to place stringent constraints on an energy dependence of the speed of light in vacuum, a manifestation of Lorentz invariance violation (LIV) predicted by some quantum gravity (QG) theories. Our results show that the 95% confidence level lower limits on the QG energy scales are $E_{\text{QG},1} > 10$ times of the Planck energy E_{Pl} for the linear, and $E_{\text{QG},2} > 6 \times 10^{-8} E_{\text{Pl}}$ for the quadratic LIV effects, respectively. Our limits on the quadratic LIV case improve previous best bounds by factors of 5–7.

PACS numbers:

I. INTRODUCTION

Lorentz invariance, the fundamental symmetry of Einstein’s relativity, has withstood very strict tests over the past century [1]. However, deviations from Lorentz invariance at energies approaching the Planck scale $E_{\text{Pl}} = \sqrt{\hbar c^5/G} \simeq 1.22 \times 10^{19}$ GeV are predicted in many quantum gravity (QG) theories seeking to unify quantum theory and general relativity [2–13]. Although any violations of Lorentz invariance (LIV) are expected to be very tiny at attainable energies $\ll E_{\text{Pl}}$, they can increase with energy and accumulate to detectable levels over large propagation distances. Astrophysical observations involving high-energy radiation and long distances are therefore suitable for carrying out sensitive tests of Lorentz invariance.

One of the manifestations of LIV can be characterised as energy-dependent modifications to the photon dispersion relation in vacuum [14]:

$$E^2 \simeq p^2 c^2 \left[1 - \sum_{n=1}^{\infty} s \left(\frac{E}{E_{\text{QG},n}} \right)^n \right], \quad (1)$$

where E and p are the energy and momentum of a photon, c

is the speed of light, $s = \pm 1$ is the “sign” of the LIV effect ($s = +1$ or $s = -1$ corresponds to the “subluminal” or “superluminal” scenarios), and $E_{\text{QG},n}$ denotes the hypothetical QG energy scale. Since the sum is dominated by the lowest-order term of the series at small energies $E \ll E_{\text{QG},n}$, only the first two leading terms ($n = 1$ or $n = 2$) are of interest for independently LIV tests. They are usually referred to as linear and quadratic LIV corrections, respectively. Taking into account only the leading LIV modification of order n , the photon group velocity is then given by

$$v(E) = \frac{\partial E}{\partial p} \approx c \left[1 - s \frac{n+1}{2} \left(\frac{E}{E_{\text{QG},n}} \right)^n \right]. \quad (2)$$

Because of the energy dependence of $v(E)$, two photons with different energies (denoted by E_h and E_l , where $E_h > E_l$) emitted simultaneously from the same source at redshift z would reach us at different times. The energy-dependent time delay due to LIV effects can be expressed as [15]

$$\Delta t_{\text{LIV}} = s \frac{n+1}{2} \frac{E_h^n - E_l^n}{E_{\text{QG},n}^n} \int_0^z \frac{(1+z')^n}{H(z')} dz', \quad (3)$$

where $H(z) = H_0 \sqrt{\Omega_m(1+z)^3 + \Omega_\Lambda}$, assuming a flat Λ CDM cosmology with Hubble constant $H_0 = 67.36 \text{ km s}^{-1} \text{ Mpc}^{-1}$, matter density parameter $\Omega_m = 0.315$, and vacuum energy density $\Omega_\Lambda = 1 - \Omega_m$ [16]. For convenience, in Eq. (3) we introduce the dimensionless LIV parameters

$$\eta_1 = s E_{\text{Pl}} / E_{\text{QG},1} \quad (4)$$

*E-mail: gmxiang@ihep.ac.cn; jjwei@pmo.ac.cn; zhiguo.yao@ihep.ac.cn; xfwu@pmo.ac.cn

and

$$\eta_2 = 10^{-15} \times s E_{\text{Pl}}^2 / E_{\text{QG},2}^2 \quad (5)$$

for linear ($n = 1$) and quadratic ($n = 2$) modifications, respectively, to replace $E_{\text{QG},1}$ and $E_{\text{QG},2}$.

It is obvious from Eq. (3) that the greatest sensitivities on the QG energy scale $E_{\text{QG},n}$ can be expected from those astrophysical sources with rapid signal variability, large distances, and high-energy emission. As the most violent explosions occurring at cosmological distances, gamma-ray bursts (GRBs) have been deemed as excellent probes for searching for the LIV-induced vacuum dispersion [14, 17–20]. Indeed, the most stringent limits to date on $E_{\text{QG},n}$, resulting from vacuum dispersion time-of-flight studies, have been obtained using the GeV emission of GRB 090510 observed by the *Fermi* Large Area Telescope (LAT). The limits set for the subluminal (superluminal) scenario are $E_{\text{QG},1} > 9.3 \times 10^{19}$ GeV ($E_{\text{QG},1} > 1.3 \times 10^{20}$ GeV) and $E_{\text{QG},2} > 1.3 \times 10^{11}$ GeV ($E_{\text{QG},2} > 9.4 \times 10^{10}$ GeV) for linear and quadratic LIV effects, respectively [19]. Based on the first detection of sub-TeV emission from GRB 190114C by the Major Atmospheric Gamma Imaging Cherenkov (MAGIC) telescopes, Ref. [21] obtained competitive lower limits on the quadratic LIV energy scale, i.e., $E_{\text{QG},2} > 6.3 \times 10^{10}$ GeV ($E_{\text{QG},2} > 5.6 \times 10^{10}$ GeV) for the subluminal (superluminal) case.

On October 9, 2022, the Large High Altitude Air Shower Observatory (LHAASO) detected more than 64,000 photons in the energy range of 0.2–7 TeV from GRB 221009A within the first 4000 s after the MeV burst trigger, recording the most energetic GRB photons ever observed [22]. This object is estimated to be located at redshift $z = 0.151$ [23, 24]. In this Letter, we study Lorentz-violating effects using the time-of-flight measurements of the unprecedentedly very-high-energy (VHE, > 100 GeV) γ -ray signal from GRB 221009A.

II. LHAASO OBSERVATIONS OF GRB 221009A

At $T_0 = 13:16:59.99$ universal time on 9 October 2022, a special long-duration GRB, numbered as GRB 221009A, was triggered by the Gamma-Ray Burst Monitor (GBM) onboard the *Fermi* satellite [25, 26]. The subsequent detection with *Fermi*-LAT made clear that it is an extraordinarily bright burst, recording the highest GRB photon energy (99.3 GeV, observed at $T_0 + 240$ s) ever detected by *Fermi*-LAT [27, 28]. The γ -ray emission of GRB 221009A was also detected by several other space missions [29], and by ground-based air shower detectors [30].

LHAASO is a new generation γ -ray and cosmic-ray observatory situated in Daocheng, China, at an elevation of approximately 4410 meters above sea level [31]. The LHAASO experiment comprises three detector arrays: the Water Cherenkov Detector Array (WCDA), the Kilometer Square Array, and the Wide Field of View Cherenkov Telescope Array. Due to the large area, wide field of view, and broad energy coverage, the LHAASO detectors are meticulously designed to delve into new frontiers of physics, including investigations into LIV, among other scientific objectives.

At the GBM trigger time, GRB 221009A was observed by LHAASO at a Zenith angle of 28.1° in the local coordinates, remaining within LHAASO's field of view for the next 6000 seconds. In the initial 4000 seconds post-trigger, LHAASO captured over 64,000 photons in the 0.2–7 TeV energy range [22]. This marks the first-ever detection of VHE emissions from a GRB in the early epoch. Given the exceptionally high photon statistics, both the light curve and energy spectrum of VHE γ rays from GRB 221009A can be clearly characterized. The intrinsic light curve in the 0.2–7 TeV energy range reveals a rapid ascent to a peak around 245 seconds, followed by a decay lasting at least 3000 seconds after the peak. This behavior can be well-described by a semi-smoothed-quadruple-broken-power-law function [22]. The intrinsic flux spectra for different time intervals are effectively fitted with a power-law function, demonstrating a slight softening evolution of the spectral index [22].

III. ANALYSIS METHODS AND RESULTS

We employ two analysis methods to investigate the LIV lags in the VHE γ -ray signals from GRB 221009A. Firstly, the cross-correlation function (CCF) is utilized to directly measure the time delays between different energy bands. The CCF method avoids any model assumptions regarding the intrinsic temporal or energy distributions of the source. Additionally, we apply the maximum likelihood (ML) method to extract energy-dependent arrival delays for the LIV analysis. The ML method is somewhat model-dependent, as it requires adopting certain light curve models to describe the combined probability of detecting a set of photons with individual energy arriving at a given time, assuming an energy-dependent time delay induced by LIV effects.

A. Cross-correlation Function Method

We segment the light curve of the count rate detected by LHAASO-WDA from GRB 221009A into ten intervals, covering the time span from 232 to 400 seconds after the GBM trigger. The segmentation is based on the number of fired cells (N_{hit}), with approximately the same number of events in each segment. The N_{hit} segments roughly correspond to different energy ranges, and the median energies for these segments are 0.354, 0.375, 0.395, 0.419, 0.457, 0.486, 0.556, 0.658, 0.843, and 1.601 TeV, respectively, considering the spectral index from [22] for the mentioned time interval. The energy-dependent light curves of GRB 221009A for the ten N_{hit} segments (denoted by Seg0–Seg9) are displayed in Fig. 1.

Time lags between the lowest energy band (Seg0) and any of the other nine high energy bands (Seg1–Seg9) can be calculated using the CCF defined as

$$F_j(\Delta t) = \frac{\sum_i R_0(t_i) R_j(t_i + \Delta t)}{\sqrt{\sum_i R_0^2(t_i) \sum_i R_j^2(t_i)}}, \quad (6)$$

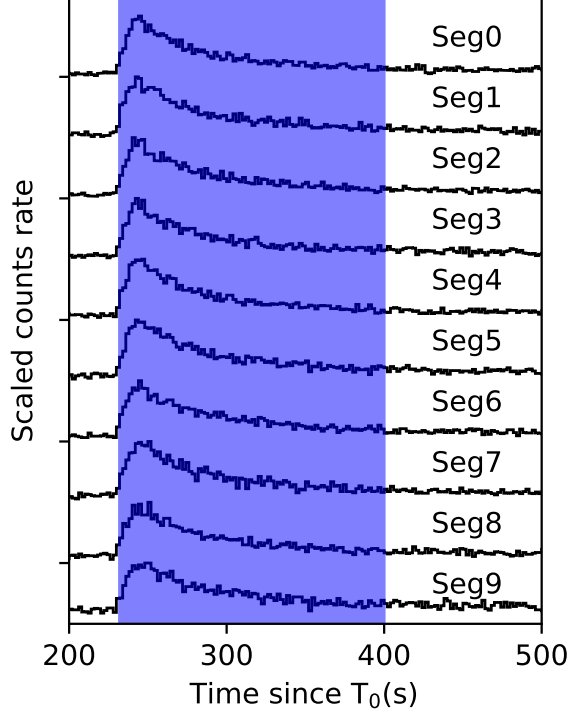


FIG. 1: Count rate light curves of GRB 221009A, as detected by LHAASO-WCDA, presented in ten N_{hit} segments. The time binning of the light curves used for analysis is 0.1 s; however, they are depicted here with 2 s intervals for clarity. The blue-marked range from 232 to 400 s after the GBM trigger T_0 is selected for calculating the time lags.

where $j = 1, 2, 3, \dots, 9$ represents the N_{hit} segment number except the first one, i is the time bin number, $R_0(t_i)$ and $R_j(t_i)$ are the rates of segment 0 and j at time bin t_i , and Δt is the time lag. A discrete analysis is performed with a time step set to 0.1 s. By fitting $F_j(\Delta t)$ around the peak with a Gaussian function, a more precise peak position Δt_j can be obtained.

Assuming that the observed time lags are primarily caused by LIV effects, we can establish a conservative lower limit on the LIV parameter η_n ($n = 1$ or 2). Utilizing the 9 pairs of CCF measurements, we conduct a global fit to constrain η_n by minimizing

$$\chi^2(\eta_n) = \sum_j \frac{[\Delta t_j - \Delta t_{\text{LIV}}(\eta_n)]^2}{\sigma^2(\Delta t_j)}, \quad (7)$$

where $\sigma(\Delta t_j)$ is the uncertainty of Δt_j , regarded as a statistical origin. This uncertainty is obtained by mocking the data (i.e., randomly sampling the histograms) for this CCF pair 1000 times, and the spread of Δt_j is chosen as the value.

In Eq. (7), the median energy of photons is selected for calculating the LIV time delay $\Delta t_{\text{LIV}}(\eta_n)$ for each N_{hit} segment. However, this approach may introduce bias since photon energies exhibit wide dispersion within each N_{hit} segment, primarily due to air shower fluctuations, and there is significant overlap in energy ranges among neighboring segments. The

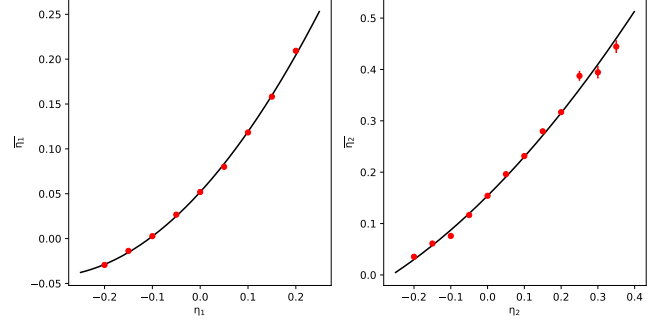


FIG. 2: Relationship between the induced LIV value of $\overline{\eta}_n$ (with $\overline{\eta}_1$ in the left panel and $\overline{\eta}_2$ in the right panel) and the input η_n (denoted as η_1 and η_2 respectively), obtained through a simulation procedure. The difference between $\overline{\eta}_n$ and η_n can be considered as the bias primarily originating from the energy overlapping of different N_{hit} segments.

following procedure is employed to estimate this bias.

The light curve of energy flux in the specified time range, as measured by LHAASO-WCDA, can be well described by a smoothed broken power-law function [22],

$$\lambda(t) \propto \left[\left(\frac{t}{t_b} \right)^{-\omega\alpha_1} + \left(\frac{t}{t_b} \right)^{-\omega\alpha_2} \right]^{-1/\omega}, \quad (8)$$

where all time-related variables are relative to a reference time $T^* = T_0 + 226$ s. Here, $\alpha_1 = 1.82$ and $\alpha_2 = -1.115$ denote the power-law indices before and after the break time $t_b = 15.37$ s, and $\omega = 1.07$ represents the sharpness of the break. The intrinsic time-resolved spectrum can be fitted with a power-law function, and the positive power-law spectral index varies with time following the expression [22]

$$\gamma(t) = a \log(t) + b, \quad (9)$$

where the unit of t is seconds, and $a = -0.135$ and $b = 2.579$. Assuming a LIV parameter η_1 or η_2 , the intrinsic light curve of energy flux can be simulated. Taking into account the attenuation of extra-galactic background lights (EBL) and utilizing the WCDA detector efficiency matrix that converts E to N_{hit} , the light curve of energy flux can be translated into ten count rate light curves, like what are shown in Fig. 1. Employing simulated light curves, the same procedure as with the data is executed, leading to the determination of the measured LIV parameters, as shown in Fig. 2. This involves iterating over various η_1 and η_2 values as input, enabling a polynomial fitting. Using the fitted function, the bias $\overline{\eta}_n - \eta_n$ for the analysis results on experimental data can be evaluated and subtracted.

Finally, employing an MCMC procedure to replicate the minimization process outlined in Eq. (7), the marginalized posterior distributions of unbiased η_n for both the linear and quadratic modifications are acquired and depicted in Fig. 3. Utilizing Eqs. (4)–(5), the best-fit values of η_n along with their uncertainties are translated into the 95% confidence level (CL) limits on the QG energy scale E_{QG} . These limits are detailed in Table I [32].

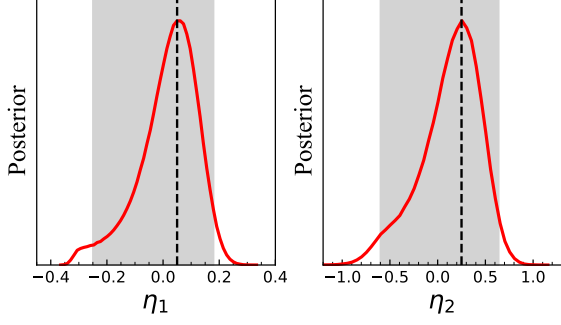


FIG. 3: Posterior probability distributions of the dimensionless LIV parameter η_n for the linear case (on the left) and the quadratic case (on the right), utilizing the CCF method. The vertical dashed lines indicate the best fits, and the shaded areas correspond to the 95% confidence intervals.

B. Maximum Likelihood Method

Another approach for inferring the LIV parameters is the maximum likelihood method. The count rate light curve, characterizing the probability of observing a photon at the number of hits N_{hit} and the arrival time t from the GRB, can be expressed as follows:

$$f(t, N_{\text{hit}}|\eta_n) = \int_0^{+\infty} \lambda [t - \Delta t_{\text{LIV}}(E, \eta_n)] \times \zeta(t) E^{-\gamma(t)} P_{\text{EBL}}(E) S(E, N_{\text{hit}}, t) dE. \quad (10)$$

Here, $\lambda [t - \Delta t_{\text{LIV}}(E, \eta_n)]$ denotes the temporal distribution of photons from the GRB, as shown in Eq. (8), after accounting for the LIV-induced time delay with parameter η_n . Additionally, $\zeta(t) = A / \int_{E_1}^{E_2} E^{1-\gamma(t)} dE$ serves as the conversion factor from energy flux (within the energy range from $E_1 = 0.3$ TeV to $E_2 = 5$ TeV) to flux coefficient, where $\gamma(t)$ represents the power-law index evolution as per Eq. (9), and A is a constant to be determined. The term $P_{\text{EBL}}(E)$ denotes the survival probability of photons subject to EBL attenuation, with the model from [34] adopted, considering a redshift $z = 0.151$. Lastly, $S(E, N_{\text{hit}}, t)$ accounts for the effective detection area of photons at energy E , with consideration for the number of hits N_{hit} and time t .

A binned Poissonian likelihood method is employed for the analysis, with a time binning set to 0.1 s and N_{hit} split into 10 segments as illustrated in Fig. 1. The background distribution, as a function of time for each N_{hit} segment, is determined using data from the same transit as the GRB, encompassing two sidereal days before and after the burst. The Poisson probability is given by

$$\mathcal{P}_{i,j} = \frac{e^{-(\mu_{b,i,j} + \mu_{s,i,j})} (\mu_{b,i,j} + \mu_{s,i,j})^{N_{\text{on},i,j}}}{N_{\text{on},i,j}!}, \quad (11)$$

where index i represents time bins, and j represents N_{hit} segments. The number of signals from the GRB $\mu_{s,i,j}$ is calculated using Eq. (10), the number of background events $\mu_{b,i,j}$ is

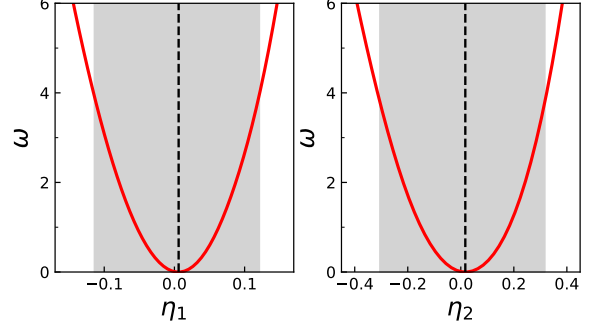


FIG. 4: Likelihood profiles resulting from the analysis with the maximum likelihood method, depicted for both linear (on the left) and quadratic (on the right) cases. The vertical dashed lines signify the best fits after bias subtraction, and the shaded areas correspond to the 95% confidence intervals.

evaluated from the polynomial fitting of the background as a function of time, and $N_{\text{on},i,j}$ is the number of observed events. The logarithmic likelihood ratio is defined as

$$\omega = -2 \ln \frac{\mathcal{L}}{\mathcal{L}_0} = -2 \sum_{i,j} \left[(\mu'_{s,i,j} - \mu_{s,i,j}) + N_{\text{on},i,j} \ln \frac{\mu_{b,i,j} + \mu_{s,i,j}}{\mu_{b,i,j} + \mu'_{s,i,j}} \right]. \quad (12)$$

This ratio is utilized for minimization to determine the LIV parameter η_n and all other light curve parameters. The reference time (T^* , see the context of Eq. (8)) and two parameters for spectral index evolution (a and b , see Eq. (9)) are fixed to the values provided in [22]. In this equation, $\mathcal{L} = \prod_{i,j} \mathcal{P}_{i,j}$ is the likelihood function, and \mathcal{L}_0 is the one for a null hypothesis that no LIV delay exists, where the number of signals corresponds to $\mu'_{s,i,j}$ through setting $\Delta t_{\text{LIV}}(E, \eta_n) = 0$ in Eq. (10). Within the minimization procedure, the profile likelihood curves for η_n can be obtained, allowing for the calculation of the error ranges or confidence levels, using the method developed in [35].

There may be biases in this approach for η_1 and η_2 , as, for instance, Eq. (10) does not fit the data well, and some of the fixed parameters used in the function are correlated with the LIV term. We conducted an analysis on 1000 shuffled data sets by randomly exchanging the time and N_{hit} information of events to decouple the correlation of time and energy. To maintain the behavior of the spectral index evolution, we locally shuffled the events in each time bin with a width of 6 seconds and reshuffled them after shifting half of the time bin. The chosen time binning for shuffling is sufficiently large, as the maximum time delay is less than 6 seconds within the energy coverage of the data for $|\eta_1| < 0.15$ or $|\eta_2| < 0.35$. The means of the 1000 best-fit values of η_n of the shuffled data are considered as the biases. The likelihood profile distributions after subtracting the biases are depicted in Fig. 4, whereas the distributions of the best-fit values for the shuffled data are in Fig. 5.

As no significant LIV time delay from GRB 221009A are

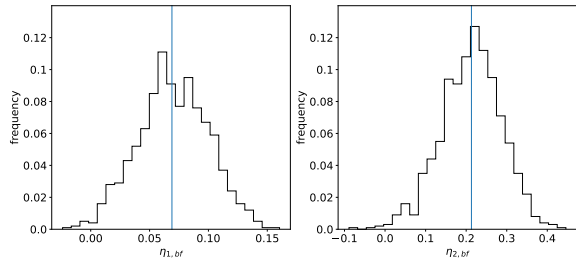


FIG. 5: Distribution of best-fit values from the shuffled data, presented for both linear (on the left) and quadratic (on the right) cases. The vertical lines indicate the means.

detected in this approach, we set upper limits for η_n by constructing 95% confidence intervals. The obtained values of η_n are subsequently used to compute the limits on the QG energy scale E_{QG} . The corresponding results are listed in Table I.

The EBL model could introduce systematic uncertainties in our analysis. To quantify this effect, we conducted two parallel comparative analyses of the GRB data, considering two extreme cases of the EBL models (corresponding to the upper and lower boundaries of the uncertainty in the EBL model in [34]). For the linear LIV effect, we observe that the EBL models would enlarge the limits by 18% in subluminal scenario and by 12% in superluminal scenario. In the case of the quadratic LIV effect, the limits would be reduced by 6% in subluminal scenario and by 5% in superluminal scenario.

IV. SUMMARY

LHAASO observed unprecedented large number of VHE γ -ray signals from the brightest GRB 221009A at the earliest epoch, marking the identification of the onset of a TeV GRB afterglow for the first time. These characteristics render this signal a unique opportunity to probe LIV in the photon sector. Utilizing both CCF and ML methods, we searched for LIV-induced lags in the arrival time of the energetic photons. In both methods, compatible limits on the LIV energy scale E_{QG} are obtained.

Our limit on the linear modification of the photon dispersion relation is $E_{QG,1} > 1.0 \times 10^{20} \text{GeV}$ ($E_{QG,1} > 1.1 \times 10^{20} \text{GeV}$), considering a subluminal (superluminal) LIV ef-

fect. This is comparable to the most constraining lower limit on $E_{QG,1}$ obtained by the GeV emission of GRB 090510 [19]. In the quadratic case, our result on the energy scale $E_{QG,2} > 6.9 \times 10^{11} \text{GeV}$ ($E_{QG,2} > 7.0 \times 10^{11} \text{GeV}$) for a subluminal (superluminal) LIV effect represents the best time-of-flight limit, improving previous bounds [19] by a factor of 5 (7).

Moreover, we emphasize that, thanks to the adoption of the true spectral time lags of bunches of high-energy photons, our constraints on $E_{QG,n}$ could be statistically robust compared to previous results of GRB 090510, which were based on the rough time lags of sparse GeV-scale photons.

Future observations of VHE prompt emission instead of afterglow from GRBs with LHAASO, MAGIC, CTA, and other detectors would further enhance sensitivity to LIV effects using vacuum dispersion (time-of-flight) tests.

Acknowledgments

We would like to thank all staff members who work at the LHAASO site above 4400 meters above sea level year-round to maintain the detector and keep the water recycling system, electricity power supply and other components of the experiment operating smoothly. We are grateful to Chengdu Management Committee of Tianfu New Area for the constant financial support for research with LHAASO data. This research work is also supported by the following grants: The National Key R&D program of China under grants 2018YFA0404201, 2018YFA0404202, 2018YFA0404203, and 2018YFA0404204, the National Natural Science Foundation of China (Nos. U1831208, 12005246, 12173039, 12321003, 12373053, and 12375108), the Strategic Priority Research Program of the Chinese Academy of Sciences (grant No. XDB0550400), the Department of Science and Technology of Sichuan Province, China No. 2021YFSY0030, Project for Young Scientists in Basic Research of Chinese Academy of Sciences No. YSBR-061, the Key Research Program of Frontier Sciences of Chinese Academy of Sciences No. ZDBS-LY-7014, the Natural Science Foundation of Jiangsu Province No. BK20221562, and in Thailand by the National Science and Technology Development Agency (NSTDA) and National Research Council of Thailand (NRCT): High-Potential Research Team Grant Program (N42A650868).

[1] V. A. Kostelecký and N. Russell, *Reviews of Modern Physics* **83**, 11 (2011), 0801.0287.
[2] V. A. Kostelecký and S. Samuel, *Phys. Rev. D* **39**, 683 (1989).
[3] G. Amelino-Camelia, J. Ellis, N. E. Mavromatos, and D. V. Nanopoulos, *International Journal of Modern Physics A* **12**, 607 (1997), hep-th/9605211.
[4] J. Ellis, N. E. Mavromatos, and D. V. Nanopoulos, *General Relativity and Gravitation* **31**, 1257 (1999), gr-qc/9905048.
[5] G. Amelino-Camelia, *Nature (London)* **418**, 34 (2002), gr-qc/0207049.
[6] J. Magueijo and L. Smolin, *Phys. Rev. Lett.* **88**, 190403 (2002),

hep-th/0112090.
[7] J. Alfaro, H. A. Morales-Técolt, and L. F. Urrutia, *Phys. Rev. D* **65**, 103509 (2002), hep-th/0108061.
[8] D. Mattingly, *Living Reviews in Relativity* **8**, 5 (2005), gr-qc/0502097.
[9] T. Li, N. E. Mavromatos, D. V. Nanopoulos, and D. Xie, *Physics Letters B* **679**, 407 (2009), 0903.1303.
[10] G. Amelino-Camelia, *Living Reviews in Relativity* **16**, 5 (2013), 0806.0339.
[11] J. D. Tasson, *Reports on Progress in Physics* **77**, 062901 (2014), 1403.7785.

TABLE I: Values for the best fits (BF) and the 95% lower (LL) and upper (UL) limits, provided for the dimensionless LIV parameter η_n using both the CCF and ML methods. Additionally, the 95% confidence level (CL) lower limits on the quantum gravity (QG) energy scale E_{QG} for the linear ($n = 1$) and quadratic ($n = 2$) cases are listed.

Method	Cross correlation function			Maximum likelihood		
	η^{LL}	η^{BF}	η^{UL}	η^{LL}	η^{BF}	η^{UL}
η_1	-0.25	0.05	0.18	-0.11	0.01	0.12
η_2	-0.60	0.25	0.64	-0.31	0.02	0.32
	superluminal		subluminal	superluminal	subluminal	
$E_{\text{QG},1}$ [10^{20} GeV]	0.5		0.7	1.1		1.0
$E_{\text{QG},2}$ [10^{11} GeV]	5.0		4.8	7.0		6.9

- [12] J.-J. Wei and X.-F. Wu, *Frontiers of Physics* **16**, 44300 (2021), 2102.03724.
- [13] P. He and B.-Q. Ma, *Universe* **8**, 323 (2022), 2206.08180.
- [14] G. Amelino-Camelia, J. Ellis, N. E. Mavromatos, D. V. Nanopoulos, and S. Sarkar, *Nature (London)* **393**, 763 (1998), astro-ph/9712103.
- [15] U. Jacob and T. Piran, *JCAP* **2008**, 031 (2008), 0712.2170.
- [16] Planck Collaboration, N. Aghanim, Y. Akrami, M. Ashdown, J. Aumont, C. Baccigalupi, M. Ballardini, A. J. Banday, R. B. Barreiro, N. Bartolo, et al., *Astron. & Astrophys.* **641**, A6 (2020), 1807.06209.
- [17] A. A. Abdo, M. Ackermann, M. Arimoto, K. Asano, W. B. Atwood, M. Axelsson, L. Baldini, J. Ballet, D. L. Band, G. Barbiellini, et al., *Science* **323**, 1688 (2009).
- [18] A. A. Abdo, M. Ackermann, M. Ajello, K. Asano, W. B. Atwood, M. Axelsson, L. Baldini, J. Ballet, G. Barbiellini, M. G. Baring, et al., *Nature (London)* **462**, 331 (2009), 0908.1832.
- [19] V. Vasileiou, A. Jacholkowska, F. Piron, J. Bolmont, C. Couturier, J. Granot, F. W. Stecker, J. Cohen-Tanugi, and F. Longo, *Phys. Rev. D* **87**, 122001 (2013), 1305.3463.
- [20] J. Ellis, R. Konoplich, N. E. Mavromatos, L. Nguyen, A. S. Sakharov, and E. K. Sarkisyan-Grinbaum, *Phys. Rev. D* **99**, 083009 (2019), 1807.00189.
- [21] V. A. Acciari, S. Ansoldi, L. A. Antonelli, A. Arbet Engels, D. Baack, A. Babić, B. Banerjee, U. Barres de Almeida, J. A. Barrio, J. Becerra González, et al. (MAGIC Collaboration), *Phys. Rev. Lett.* **125**, 021301 (2020), URL <https://link.aps.org/doi/10.1103/PhysRevLett.125.021301>.
- [22] LHAASO Collaboration, Z. Cao, F. Aharonian, Q. An, A. Axikegu, L. X. Bai, Y. X. Bai, Y. W. Bao, D. Bastieri, X. J. Bi, et al., *Science* **380**, 1390 (2023), 2306.06372.
- [23] A. de Ugarte Postigo, L. Izzo, G. Pugliese, D. Xu, B. Schneider, J. P. U. Fynbo, N. R. Tanvir, D. B. Malesani, A. Saccardi, D. A. Kann, et al., *GRB Coordinates Network* **32648**, 1 (2022).
- [24] D. B. Malesani, A. J. Levan, L. Izzo, A. de Ugarte Postigo, G. Ghirlanda, K. E. Heintz, D. A. Kann, G. P. Lamb, J. Palmerio, O. S. Salafia, et al., arXiv e-prints arXiv:2302.07891 (2023), 2302.07891.
- [25] P. Veres, E. Burns, E. Bissaldi, S. Lesage, O. Roberts, and Fermi GBM Team, *GRB Coordinates Network* **32636**, 1 (2022).
- [26] S. Lesage, P. Veres, M. S. Briggs, A. Goldstein, D. Kocevski, E. Burns, C. A. Wilson-Hodge, P. N. Bhat, D. Huppenkothen, C. L. Fryer, et al., arXiv e-prints arXiv:2303.14172 (2023), 2303.14172.
- [27] E. Bissaldi, N. Omodei, M. Kerr, and Fermi-LAT Team, *GRB Coordinates Network* **32637**, 1 (2022).
- [28] R. Pillera, E. Bissaldi, N. Omodei, G. La Mura, F. Longo, and Fermi-LAT team, *GRB Coordinates Network* **32658**, 1 (2022).
- [29] S. Dichiara *et al.*, *GRB Coordinates Network* **32632**, 1 (2022); H. A. Krimm *et al.*, *GRB Coordinates Network* **32688**, 1 (2022); A. Ursi *et al.*, *GRB Coordinates Network* **32650**, 1 (2022); G. Piano *et al.*, *GRB Coordinates Network* **32657**, 1 (2022); D. Gotz *et al.*, *GRB Coordinates Network* **32660**, 1 (2022); H. Xiao *et al.*, *GRB Coordinates Network* **32661**, 1 (2022); L. Lapshov *et al.*, *GRB Coordinates Network* **32663**, 1 (2022); D. Frederiks *et al.*, *GRB Coordinates Network* **32668**, 1 (2022); D. Frederiks *et al.*, arXiv e-prints arXiv:2302.13383 (2023), 2302.13383; J. Ripa *et al.*, *GRB Coordinates Network* **32685**, 1 (2022); J. Ripa *et al.*, arXiv e-prints arXiv:2302.10047 (2023), 2302.10047; L. J. Mitchell *et al.*, *GRB Coordinates Network* **32746**, 1 (2022); J. C. Liu *et al.*, *GRB Coordinates Network* **32751**, 1 (2022); Z.-H. An *et al.*, arXiv e-prints arXiv:2303.01203 (2023), 2303.01203; K.-K. Duan *et al.*, *GRB Coordinates Network* **32973**, 1 (2022).
- [30] Y. Huang *et al.*, *GRB Coordinates Network* **32677**, 1 (2022); D. D. Dzhabpuev *et al.*, *GRB Coordinates Network* **15669**, 1 (2022).
- [31] X.-H. Ma, Y.-J. Bi, Z. Cao, M.-J. Chen, S.-Z. Chen, Y.-D. Cheng, G.-H. Gong, M.-H. Gu, H.-H. He, C. Hou, et al., *Chinese Physics C* **46**, 030001 (2022).
- [32] Similar bounds were given in [33], which we received while working on this paper.
- [33] T. Piran and D. D. Ofengeim, arXiv e-prints arXiv:2308.03031 (2023), 2308.03031.
- [34] A. Saldana-Lopez, A. Domínguez, P. G. Pérez-González, J. Finke, M. Ajello, J. R. Primack, V. S. Paliya, and A. Desai, *Mon. Not. R. Astron. Soc.* **507**, 5144 (2021), 2012.03035.
- [35] W. A. Rolke, A. M. López, and J. Conrad, *Nuclear Instruments and Methods in Physics Research A* **551**, 493 (2005), physics/0403059.